ACS OMEGA

http://pubs.acs.org/journal/acsodf

Article

Stability Evaluation of Candidate Precursors for Chemical Vapor Deposition of Hafnium Diboride (HfB_2)

Jessica M. Rimsza,* Samuel C. B. Chackerian, Timothy J. Boyle, and Bernadette A. Hernandez-Sanchez

Cite This: *ACS Omega* 2021, 6, 11404−11410

Read Online

ACCESS | Metrics & More | Article Recommendations | Supporting Information

ABSTRACT: Alternative candidate precursors to $[Hf(BH_4)_4]$ for low-temperature chemical vapor deposition of hafnium diboride (HfB_2) films were identified using density functional theory simulations of molecules with the composition $[Hf(BH_4)_2L_2]$, where L = −OH, −OMe, −O-*t*-Bu, $-NH_2$, −N═C═O, $-N(Me)_2$, and $-N(CH_2)_5NH_2$ (1-piperidin-2-amine referred to as Pip2A). Disassociation energies (E_D), potential energy surface (PES) scans, ionization potentials, and electron affinities were all calculated to identify the strength of the Hf−L bond and the potential reactivity of the candidate precursor. Ultimately, the low E_D (2.07 eV) of the BH_4 ligand removal from the Hf atom in $[Hf(BH_4)_4]$ was partially attributed to an intermediate state where $[Hf(BH_4)_3(H)]$ and BH_3 is formed. Of the candidate precursors investigated, three exhibited a similar mechanism, but only −Pip2A had a PES scan that indicated binding competitive with $[Hf(BH_4)_4]$, making it a viable candidate for further study.

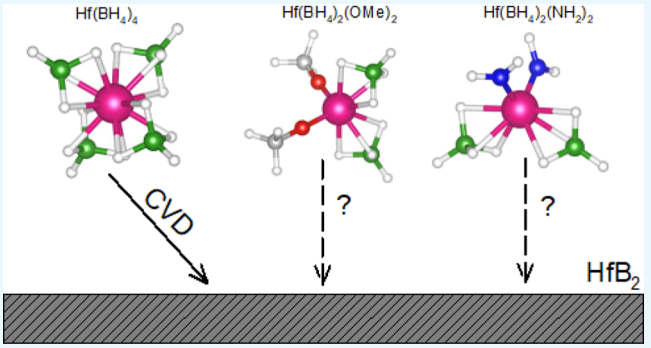

INTRODUCTION

Hafnium diboride (HfB_2) is an ultra-high-temperature ceramic that exhibits desirable properties such as high hardness and wear resistance.[1−3] Due to the favorable tribological properties and thermal stability, the vapor growth of HfB_2 thin films on nonconformal surfaces is particularly attractive for probe-based storage,[4] micro electromechanical systems,[5] magnetic storage devices,[6] and as a component in low-power gas sensors.[7] Therefore, it is not surprising that numerous methods have been developed to generate HfB_2 thin films. In particular, sputtering[8] or chemical vapor deposition (CVD) processes[9] have garnered significant attention due to the conformal coatings produced; however, control over the final film stoichiometry and high internal stresses have led to the investigation of numerous precursors. Of these, hafnium borohydride $[Hf(BH_4)_4]$[5,10−19] has come to the forefront, but the processing must be highly controlled to form uniform and dense films.[12,20] This is often undertaken using background gases, such as NH_3, as an inhibitor to block reactive sites on the surface[14] and plasma-based surface treatments to improve reactivity.[13] These studies indicate that an understanding of the precursor stability and properties during vapor processing is needed to control film quality.

An avenue to generate improved HfB_2 films that remains largely unexplored is the development of new HfB_2 CVD precursors that would allow for low-temperature deposition, without the use of background gases. Atomistic modeling can provide data on a suite of currently unsynthesized precursors to direct ongoing experimental efforts in targeting chemistries toward new viable precursor options. This approach has been previously used to optimize CVD and atomic layer deposition (ALD) of Cu,[21] Ti,[22] and transition-metal oxide films.[23] Currently, most computational studies of HfB_2 have been density functional theory (DFT) investigations focused on exploring the electrical, mechanical, and thermal properties of HfB_2.[24−27] Additionally, DFT calculations have been used to study surface interactions, such as HfB_2 and SiH_4[28] and Hf(B−M) (M = Li−Ne).[29] However, these periodic DFT investigations only provide insight into the structure and surface reactivity of HfB_2 after it has been formed, while computational investigations of $[Hf(BH_4)_4]$ are less common, focusing on the geometric[30,31] and electronic structures.[32] These studies do not explore how manipulating the $[Hf(BH_4)_4]$ molecule may allow for improvements in HfB_2 deposition.

Herein, DFT gas-phase cluster calculations were used to investigate (i) the properties of the $[Hf(BH_4)_4]$ precursor that make it well suited to HfB_2 deposition and (ii) which molecular precursors, modeled after $[Hf(BH_4)_4]$ derivatives, may exhibit similar or improved properties for low-temperature

Received: January 21, 2021
Accepted: April 13, 2021
Published: April 23, 2021

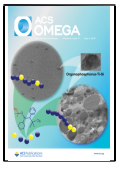

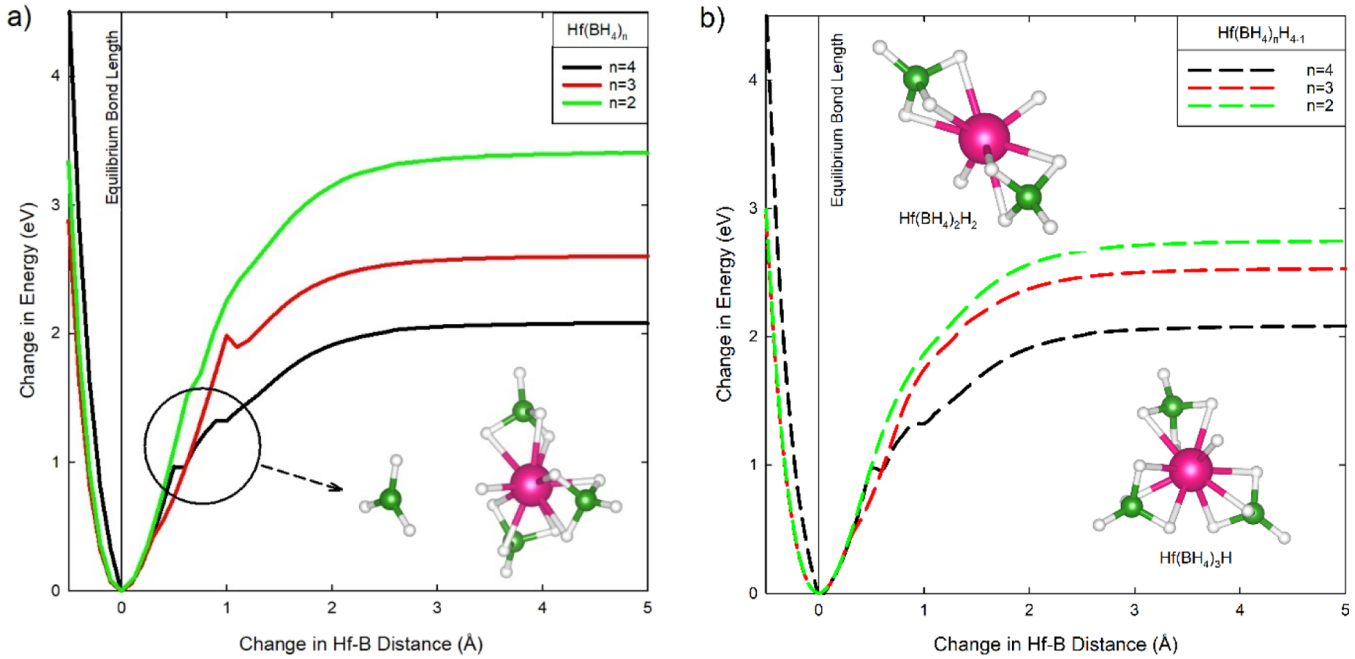

Figure 1. Energy and snapshots of (a) $[Hf(BH_4)_n]$ (n = 4−2) PES scans, and the inset shows the intermediate state of $[Hf(BH_4)_3(H)]$ and BH_3 and (b) energy and snapshots of $[Hf(BH_4)_nH_{4-n}]$ (n = 4−2) and insets of $Hf(BH_4)_3H$ and $Hf(BH_4)_2H_2$. Atom colors: Hf (pink), B (green), and H (white).

CVD processing. This study focused on simulated candidate precursors with the composition $[Hf(BH_4)_2L_2]$ and a 1:2 Hf/B ratio to optimize the deposition of a HfB_2 stoichiometric composition. While an ideal CVD precursor requires a balance of several different properties (i.e., reactivity, deposition temperature, long-term stability, reaction type, and ability to scale up), this study focused on the strength of the Hf−ligand (Hf−L) interaction, the disassociation energy (E_D), and the reactivity [ionization potential (IP), electron affinity (EA)] as representative values for the selection of viable precursors. The ideal precursor would have an E_D that is positive, indicating that the ligand binds with the Hf, but the energy is low enough that it could be easily removed.

RESULTS AND DISCUSSION

During CVD processing, the excess $-BH_4$ ligands must be removed to generate a stoichiometric HfB_2 film.[33] Ideally this would proceed from the following reaction

$$[Hf(BH_4)_4] \rightarrow HfB_2 + B_2H_6 + 5H_2 \quad (1)$$

To mimic this process, $-BH_4$ ligands were systematically removed from the $[Hf(BH_4)_4]$ molecule, which allowed for the comparison of the relative binding strength of each $-BH_4$ ligand to the Hf atom.

Mechanisms of $[Hf(BH_4)_4]$ Disassociation. Initially, the coordination structure of $[Hf(BH_4)_4]$ was found to be tetrahedral in terms of B coordination [109° for the B−Hf−B angle (Table S1)], which is consistent with the neutron diffraction data reported by Borisenko et al.[31] The removal of the first $-BH_4$ ligands led to a trigonal-planar geometry for the resulting $[Hf(BH_4)_3]$ and then to linear for $[Hf(BH_4)_2]$. Complete structural parameters and additional structural information are available in the Supporting Information section (Table S2) along with snapshots of the structures (Figure S1).

As expected, the Hf−B bond decreases from 2.28 Å to 2.26 Å to 2.20 Å as the BH_4 moieties are removed. The Hf−B−H angles show a similar trend, decreasing as the BH_4 moieties are removed from 66.85° to 66.19° to 65.83°. Potential energy surface (PES) scans as shown in Figure 1 reveal that the Hf−B interaction decreases as the number of ligands increases (2.0 eV to 2.58 eV to 3.52 eV), indicating greater dissociation energy upon loss of the ligands. Upon removal of a $-BH_4$ moiety, a H atom remains on the Hf to maintain four-fold coordination (Figure 1a inset). Therefore, the E_D was calculated for two conditions where (i) a $-BH_3$ moiety is removed and the H atom remains and coordinates the Hf atom and (ii) the entire $-BH_4$ ligand is removed. When the H atom remains, the E_D is lowered by 2.0−2.3 eV. This H atom-based mechanism is depicted in the inset in Figure 1a.

In Figure 1b, the PES is calculated for the $[Hf(BH_4)_nH_{4-n}]$ structures, which assumes that the Hf atom remains four coordinated with n BH_4 moieties and $4n$ H atoms for n = 4−2. These structures exhibit overall lower PES values than if the $-BH_4$ moiety is removed completely. Therefore, the presence of the remaining H atoms facilitates the dissociation of the $-BH_4$ moiety.

Additionally, the EA and the IP were calculated for each candidate precursor (Table 1) and provide insight into molecule stability. While the +4 oxidation state is by far the most commonly observed for Hf,[34] other oxidation states have

Table 1. Structure and Properties of $[Hf(BH_4)_n]$

$[Hf(BH_4)_n]$ (n)	Hf···B distance (Å)	E_D (eV)		IP (eV)	EA (eV)
		BH_3 + H[a]	BH_4[b]		
4	2.278	2.07	4.26	10.108	−0.912
3	2.257	2.58	4.59	7.395	−0.919
2	2.203	3.52	5.68	7.607	−0.929

[a]H atom remains coordinated to the central Hf atom and BH_3 is lost (intermediate state). [b]Complete removal of the $-BH_4$ ligand.

https://doi.org/10.1021/acsomega.1c00391
ACS Omega 2021, 6, 11404−11410

been reported, including +3, +2, and 0.[35−37] The negative EA of the $[Hf(BH_4)_n]$ precursors suggest that the Hf atom may be equally stable in a +3 or a +2 configuration, allowing for a lower energy transition to a new Hf−B molecule coordinated by only three $-BH_4$ ligands (with or without a coordinating H atom).

Non-reactive Disassociation of Candidate HfB_2 Precursors. Systematic variation of the Hf−L bond was performed to explore stability and potential precursor development. Here, the composition of $[Hf(BH_4)_2L_2]$ and a 1:2 Hf/B ratio was used to optimize the deposition of a HfB_2 stoichiometric composition. Both O- and N-containing ligands were evaluated for suitability as potential modifiers to $Hf-BH_4$ precursors as $[Hf(BH_4)_2L_2]$ for HfB_2 deposition. The exploration of O-containing ligands was motivated by precursors used for ALD of HfO_2, which include hafnium alkoxides, $[Hf(OR)_4]$.[38,39] To elucidate the role of the Hf−O bond in candidate precursors, three oxygen-based ligands [hydroxide (−OH), methoxide (−OMe), and *tert*-butoxide (−O-*t*-Bu)] were evaluated. Additionally, previous reports of stable Hf-based complexes included N-based ligands, such as the Hf atom coordinated by pyridyl-amide ligand,[40] ethyl, methyl amine,[41,42] and diethyl amine.[43] Therefore, four N-based ligands as a potential replacement for the $-BH_4$ were evaluated, including amide ($-NH_2$), isocyanato (−N═C═O), dimethylamine $-N(Me)_2$, and 1-piperidin-2-amine (−Pip2A). Snapshots of all potential gas-phase molecular structures are included in Figures S2 and S3.

For candidate precursors that employed a simple ligand (−OH, $-NH_2$, and $-NMe_2$), no intermediate states were found along the PES scan (Figure 2) as noted by the smooth curve, and energies quickly exceeded the strength of the Hf−BH_4 interaction. This indicates that these $[Hf(BH_4)_2L_2]$ molecules are more stable than the original $[Hf(BH_4)_4]$ precursor and thus do not improve the potential decomposition route. There also does not seem to be a significant trend between O- or N-based ligands since they all contain similar levels of complexity (−OH vs $-NH_2$) with comparable E_D values.

Interestingly, of the seven candidate ligands investigated, −Pip2A exhibits the E_D values most like the $[Hf(BH_4)_4]$ precursor. Additionally, $[Hf(BH_4)_2(Pip2A)_2]$ has a lower IP than $[Hf(BH)_4)_4]$ which suggests that the entire molecule may be slightly more volatile than the current $[Hf(BH)_4)_4]$ precursor. It is of note that the IP and the EA of the candidate precursors do not, on their own, provide a clear consensus on which are most likely to replicate the properties of $[Hf(BH_4)_4]$. Generally, the EA/IP values for the $[Hf(BH_4)_2L_2]$ candidate precursors in Table 2 mimic that of the parent compound, and a comparable E_D appears to be more critical in the selection of an alternative. However, despite the similarities of the EA and IP of the −OH, −OMe, and −N═C═O modifiers, the differences in E_D and PES scans indicate that these three ligands are not promising alternatives to $[Hf(BH_4)_2L_2]$.

Table 2. Hf···L Distances, E_D, IP, and EA for $Hf(BH_4)_2L_2$

Ligand	Hf−L dist. (Å)	E_D (eV)	IP (eV)	EA (eV)
BH_4	2.278	2.07[a]	10.108	−0.912
OH	1.901	12.44	10.554	0.161
OMe	1.890	11.02	9.442	0.262
O-t-Bu	1.889	11.28	8.906	0.236
NH_2	2.008	11.87	8.364	0.103
N═C═O	2.008	9.37	10.22	−0.955
NMe_2	2.017	19.85	7.220	0.050
Pip2A	2.073	3.76	6.389	0.537

[a]H atom remains coordinated to the central Hf atom and BH_3 is lost (intermediate state, Figure 1).

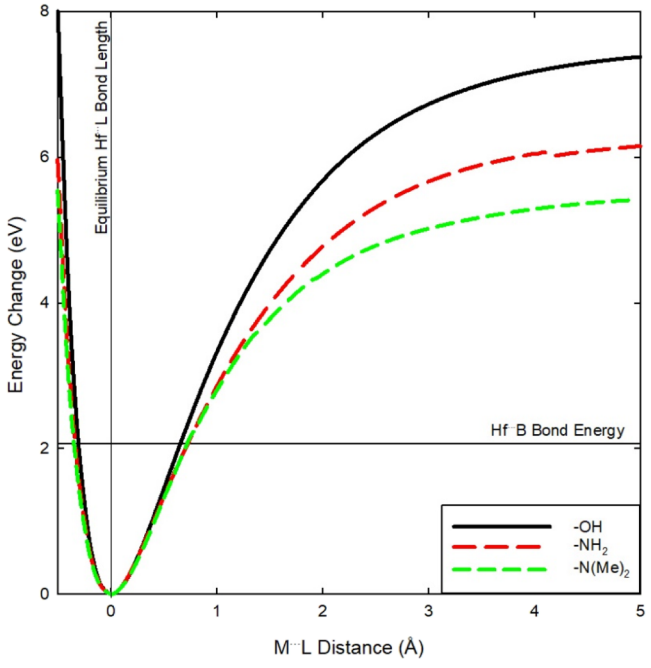

Figure 2. PES scan of $[Hf(BH_4)_2L_2]$ with L = −OH, $-NH_2$, and $-NMe_2$.

Reactive Disassociation of Candidate HfB_2 Precursors. While the E_D captures the thermodynamic stability of the candidate precursors, energy barriers and transition states identify the energy required for ligands to dissociate from the Hf atom, providing insight into the kinetic process. Four of the ligands investigated (−OMe, −O-*t*-Bu, −N═C═O, and −Pip2A) exhibit reactions during the PES scan, and these structures were used to identify the first-order transition states. The complete PES scans are included in the Supporting Information (Figure S5), while Figures 3 and 4 include snapshots of the initial and final gas-phase structures and the calculated transition states. Total energies, imaginary frequencies, and coordination structures of the transition states are included in the Supporting Information (Table S4).

For OMe, simulations indicate that a H atom remains to satisfy the 4-fold coordination of the Hf atom (Hf−OMe = 4.97 Å). For the O-*t*-Bu complex, a transition state forms, where a methyl group is instead transferred to the Hf metal center (Figure 3). The large change in energy for these two candidate precursors suggests that other O-based ligands with *β*-H may facilitate tailored decomposition pathways for the production of HfB_2.

In contrast, the $-NMe_2$ derivative did not exhibit similar ligand transfer. While the loss of the −H or $-CH_3$ from the removed ligand creates a clear energy barrier (2.78 eV for −OMe; 3.41 eV for −O-*t*-Bu), the E_D value is still not below the bond strength for the BH_4 moieties. Further exploration of the many, varied alkyl amines may be warranted, but potential precursors are less likely based on these results.

https://doi.org/10.1021/acsomega.1c00391
ACS Omega 2021, 6, 11404−11410

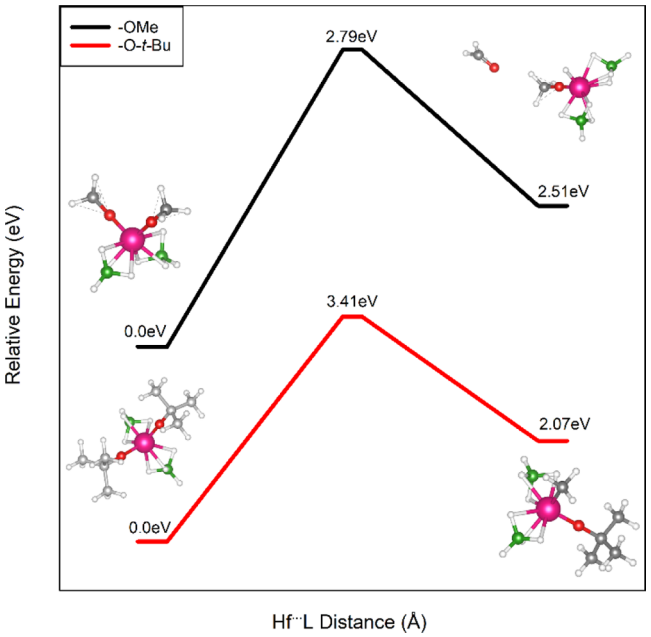

Figure 3. Energy and snapshots of $[Hf(BH_4)_2(OMe)_2]$ and $[Hf(BH_4)_2(O\text{-}t\text{-}Bu)_2]$ PES scan. Colors: Hf (pink), B (green), H (white), O (red), and C (gray).

The −N═C═O ligand exhibits significant energy variation along the PES scan due to differences in bonding as the Hf−N distance is increased (Figure 4). First, at a Hf−N bond extension of 1.0−3.0 Å, the complete −N═C═O molecule disassociates from the Hf atom. As the N═C═O diffuses away from the Hf atom, it appears to rotate and a new bond is formed between the Hf and the O atoms of the N═C═O. At a Hf···N distance of ∼3.5 Å, the N═C═O molecule inverts its bonding mode to form a Hf−O−C═N ligand. Snapshots of the different structures are included in Figure 4. At distances beyond 3.5 Å, the Hf−O bond is stretched until complete disassociation occurs. It is worth noting that these simulations are performed in a vacuum, and the presence of other gaseous molecules may react with sites in the ligand as it is removed, changing the likelihood of forming these structures. The linear structure of the −N═C═O ligand is markedly different from the 3-fold symmetry and steric bulk of the −OMe and −O-*t*-Bu ligands. The smaller steric of the −N═C═O ligand and its ability for O or N to coordinate with the Hf atom allows for these unusual transition states.

The −Pip2A ligand also exhibits an intermediate state. During the PES scan, the −═Pip2A molecule is removed from the Hf with an energy barrier of 0.34 eV. Additionally, the H from the cycloalkane remains to coordinate the Hf atom, maintaining the high coordination number. This demonstrates that a combination of the same mechanisms noted for the −OMe and −O-*t*-Bu structure can also occur on larger molecules, making them candidates for further reduction of the energy barrier for Hf−L removal and lowering the energy for CVD of HfB_2 via alternative precursors.

SUMMARY AND CONCLUSIONS

DFT simulations of potential alternative precursors to hafnium borohydride $[Hf(BH_4)_4]$ for CVD production of HfB_2 precursors were explored. For this study, modification of the standard precursor was evaluated as $[Hf(BH_4)_2(L)_2]$ in order to facilitate the deposition of HfB_2 materials. Both O-based ligands (−OH, −OMe, and−O-*t*-Bu) and N-based ligands ($-NH_2$, −N═C═O, $-NMe_2$, and −Pip2A) were investigated. It was elucidated that the steric bulk combined with the decomposition pathway of the ligand impacted the disassociation energy. Specifically, during removal of the BH_4 ligand from the $[Hf(BH_4)_4]$ precursor, hydrogen remained with the Hf atom to maintain four-fold coordination, while a BH_3 is removed to react with atmospheric constituents. The same mechanism was seen in the $[Hf(BH_4)_2(OMe)_2]$ and $[Hf(BH_4)_2(PiP2A)_2]$ precursors. In addition, there is a general trend of lower energies obtained as the steric bulk of the ligand increases (seen by E_D of 3.8 eV for −Pip2A the ligand). Based on these results, larger ligands with loosely bound hydrogens seem to be the most promising alternatives to $[Hf(BH_4)_4]$. As

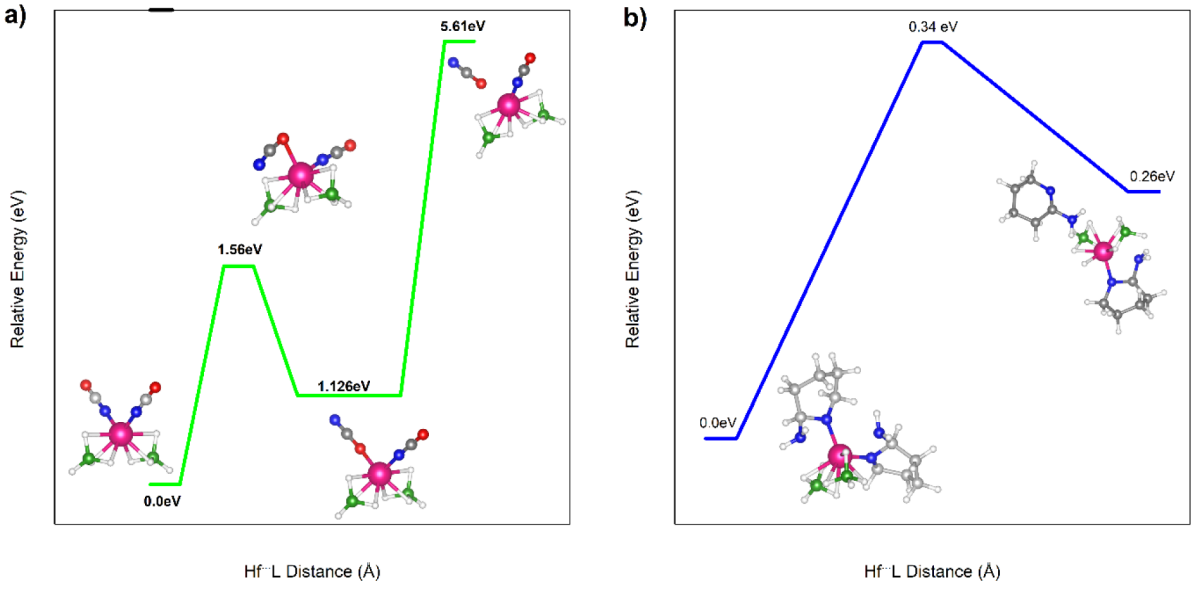

Figure 4. Energy and snapshots of (a) $[Hf(BH_4)_2(NCO)_2]$ and (b) $[Hf(BH_4)_2(Pip2A)_2]$ PES scan. Colors: Hf (pink), B (green), H (white), O (red), C (gray), and N (blue).

https://doi.org/10.1021/acsomega.1c00391
ACS Omega 2021, 6, 11404−11410

an example, the lowest energy barrier among the candidate ligands investigated was for the $[Hf(BH_4)_2(Pip2A)_2]$ molecule, which benefits from both steric effects and from a loosely bound H atom to maintain Hf coordination. Future work will focus on the synthesis of these candidate precursors, along with testing for their use in the deposition of stoichiometric HfB_2 films via CVD processes.

COMPUTATIONAL SECTION

Gas-phase electronic structure calculations were performed on $[Hf(BH_4)_4]$ and additional potential candidate HfB_2 precursors. All calculations were performed using Gaussian 09[44] with the hybrid exchange-correlation functional PBE0, a version of the Perdew, Burke, and Ernzerhof (PBE) exchange-correlation functional[45] hybridized by Adamo.[46] The functional PBE0 was chosen because it most closely matched experimental structures of $[Hf(BH_4)_4]$ (see Supporting Information, Table S1). The LANL2DZ basis set was used only on Hf atoms;[47] all other atoms were described using a 6-31G(d,p) basis set. The LANL2DZ basis set includes a scalar relativistic correction that has been previously applied to Hf-based molecules, resulting in agreement with experimental structures.[40,41,48] $[Hf(BH_4)_4]$ and additional candidate HfB_2 precursors were generated in Materials Studio[49] and were optimized in unconstrained and unrestricted DFT calculations. All molecules were optimized in the singlet state. Metrical data for the $[Hf(BH_4)_4]$ precursors matched published data. Initial coordinates, final coordinates, and coordinates for transition states are reported in the Supporting Information.

Following the relaxation of the proposed precursor, the vertical adiabatic EA and IP values were calculated to provide insight into the reactivity of the molecules. EA is the change in energy of the negatively charged molecule, with IP as the opposite case, or the energy of a positively charged molecule. Past investigations of IP and EA using DFT methods have found good agreement between experimental and computational values.[50]

E_D data was collected for complete disassociation of the $[Hf(BH_4)_2L_2]$ structure and the ligand to identify a thermodynamic drive for $Hf(BH_4)_2L_2$ decomposition. E_D data was calculated by removing the L-ligand from the $[Hf(BH_4)_2L_2]$ structure and separately relaxing the $[Hf(BH_4)_2L]$ moiety and the ligand. E_D was calculated as the difference between the complete precursor (E_P), the energy of the ligand (E_L), and the energy of the precursor without the fourth ligand (E_{P-L})

$$E_D = (E_{P-L} + E_L) - E_P \quad (2)$$

Negative E_D values indicate a thermodynamic drive to decompose the bond, while a positive E_D value indicates that the separation of the ligand from the Hf atom is not energetically favorable and that energy will need to be supplied to remove the ligand.

While the E_D data provides the thermodynamic drive for decomposition, it does not include the presence of any energy barriers, nor is there any examination of possible reactions that could happen as the precursor decomposes. Therefore, PES scans were performed to identify the strength of the Hf···ligand (Hf−L) interaction and the presence of intermediate states during disassociation. The Hf···L interatomic distance of interest, either Hf···B, Hf−O, or Hf−N, was stretched by 0.05−0.1 Å, and then the structure was relaxed. No other constraints were placed on the system during relaxation. In several cases, chemical reactions were found to occur along the PES. In these cases, a transition-state search was performed to identify the energy barrier associated with the reaction. Stationary points were identified, and the character of each point was identified to be a first-order saddle point by harmonic vibrational frequencies using the same level of theory. To identify each saddle point, intrinsic reaction coordinate calculations were performed. Geometry parameters of the resulting structure were optimized and are reported as transition states.

The E_D values, PES scans, and transition states provide a simplified basis for comparing the energy required to decompose the proposed precursor. Using computational methods to separate out likely precursor candidates will assist in streamlining the experimental synthesis of new precursors for low-temperature HfB_2 deposition.

ASSOCIATED CONTENT

Supporting Information

The Supporting Information is available free of charge at https://pubs.acs.org/doi/10.1021/acsomega.1c00391.

Basis set dependence of the geometric structure of $Hf(BH_4)_4$, change in geometric parameters for $Hf(BH_4)_4$, $Hf(BH_4)_3$, and $Hf(BH_4)_2$ and a comparison with published experimental data, total energy and imaginary frequencies of all reported first-order transition states, snapshots of optimized geometries of $Hf(BH_4)_4$, $Hf(BH_4)_3$, $Hf(BH_4)_2$, $Hf(BH_4)_2OH_2$, $Hf(BH_4)_2(OMe)_2$, $Hf(BH_4)_2(O\text{-}t\text{-}Bu)_2$, $Hf(BH_4)_2(NH_2)_2$, $Hf(BH_4)_2(NCO)_2$, and $Hf(BH_4)_2(Pip2A)_2$, and raw PES data for $Hf(BH_4)_2L_2$ with L = −OME, −O-*t*-Bu, −N=C=O, and −Pip2A are reported, along with *xyz* coordinates for all initial, final, and transition-state structures (PDF)

AUTHOR INFORMATION

Corresponding Author

Jessica M. Rimsza − *Geochemistry Department, Sandia National Laboratories, Albuquerque, New Mexico 87106, United States;* orcid.org/0000-0003-0492-852X; Phone: (505)284-3389; Email: jrimsza@sandia.gov

Authors

Samuel C. B. Chackerian − *Geochemistry Department, Sandia National Laboratories, Albuquerque, New Mexico 87106, United States*

Timothy J. Boyle − *Advanced Materials Laboratory, Sandia National Laboratories, Albuquerque, New Mexico 87106, United States;* orcid.org/0000-0002-1251-5592

Bernadette A. Hernandez-Sanchez − *Advanced Materials Laboratory, Sandia National Laboratories, Albuquerque, New Mexico 87106, United States*

Complete contact information is available at: https://pubs.acs.org/10.1021/acsomega.1c00391

Notes

The authors declare no competing financial interest.

ACKNOWLEDGMENTS

The authors would like to thank P. Salinas and N. Padilla of Sandia National Laboratories for helpful discussions. This work was funded in part by the Laboratory Directed Research

& Development (LDRD) program and by the Office of Naval Research Program under contract # N00014-20-IP00044 and approved for release reference DCN 43-7208-20. Sandia National Laboratories is a multimission laboratory managed and operated by National Technology and Engineering Solutions of Sandia, LLC., a wholly owned subsidiary of Honeywell International, Inc., for the U.S. Department of Energy's National Nuclear Security Administration under contract DE-NA0003525. This paper describes objective technical results and analysis. Any subjective views or opinions that might be expressed in the paper do not necessarily represent the views of the U.S. Department of Energy or the United States Government.

REFERENCES

(1) Dub, S. N.; Goncharov, A. A.; Ponomarev, S. S.; Filippov, V. B.; Tolmacheva, G. N.; Agulov, A. V. Mechanical properties of HfB 2.7 nanocrystalline thin films. *J. Superhard Mater.* **2011**, *33*, 151−158.
(2) Chatterjee, A.; Kumar, N.; Abelson, J. R.; Bellon, P.; Polycarpou, A. A. Nanowear of hafnium diboride thin films. *Tribol. Trans.* **2010**, *53*, 731−738.
(3) Chatterjee, A.; Kumar, N.; Abelson, J. R.; Bellon, P.; Polycarpou, A. A. Nanoscratch and nanofriction behavior of hafnium diboride thin films. *Wear* **2008**, *265*, 921−929.
(4) Tayebi, N.; Yanguas-Gil, A.; Kumar, N.; Zhang, Y.; Abelson, J. R.; Nishi, Y.; Ma, Q.; Rao, V. R. Hard HfB_2 tip-coatings for ultrahigh density probe-based storage. *Appl. Phys. Lett.* **2012**, *101*, 091909.
(5) Jayaraman, S.; Gerbi, J. E.; Yang, Y.; Kim, D. Y.; Chatterjee, A.; Bellon, P.; Girolami, G. S.; Chevalier, J. P.; Abelson, J. R. HfB_2 and Hf−B−N hard coatings by chemical vapor deposition. *Surf. Coating. Technol.* **2006**, *200*, 6629−6633.
(6) Chatterjee, A.; Jayaraman, S.; Gerbi, J. E.; Kumar, N.; Abelson, J. R.; Bellon, P.; Polycarpou, A. A.; Chevalier, J. P. Tribological behavior of hafnium diboride thin films. *Surf. Coat. Technol.* **2006**, *201*, 4317−4322.
(7) Solzbacher, F.; Imawan, C.; Steffes, H.; Obermeier, E.; Eickhoff, M. A new SiC/HfB_2 based low power gas sensor. *Sens. Actuators, B* **2001**, *77*, 111−115.
(8) Wuu, D. S.; Lee, M. L.; Lin, T. Y.; Horng, R. H. Characterization of hafnium diboride thin film resistors by rf magnetron sputtering. *Mater. Chem. Phys.* **1996**, *45*, 163−166.
(9) Rice, G. W.; Woodin, R. L. Zirconium borohydride as a zirconium boride precursor. *J. Am. Ceram. Soc.* **1988**, *71*, C-181−C-183.
(10) Yang, Y.; Jayaraman, S.; Kim, D. Y.; Girolami, G. S.; Abelson, J. R. CVD growth kinetics of HfB_2 thin films from the single-source precursor Hf $(BH_4)_4$. *Chem. Mater.* **2006**, *18*, 5088−5096.
(11) Jayaraman, S.; Gerbi, J. E.; Yang, Y.; Kim, D. Y.; Chatterjee, A.; Bellon, P.; Girolami, G. S.; Chevalier, J. P.; Abelson, J. R. HfB_2 and Hf−B−N hard coatings by chemical vapor deposition. *Surf. Coat. Technol.* **2006**, *200*, 6629−6633.
(12) Babar, S.; Kumar, N.; Zhang, P.; Abelson, J. R.; Dunbar, A. C.; Daly, S. R.; Girolami, G. S. Growth inhibitor to homogenize nucleation and obtain smooth HfB_2 thin films by chemical vapor deposition. *Chem. Mater.* **2013**, *25*, 662−667.
(13) Kumar, N.; Yanguas-Gil, A.; Daly, S. R.; Girolami, G. S.; Abelson, J. R. Remote plasma treatment of Si surfaces: Enhanced nucleation in low-temperature chemical vapor deposition. *Appl. Phys. Lett.* **2009**, *95*, 144107.
(14) Kumar, N.; Noh, W.; Daly, S. R.; Girolami, G. S.; Abelson, J. R. Low Temperature Chemical Vapor Deposition of Hafnium Nitride−Boron Nitride Nanocomposite Films. *Chem. Mater.* **2009**, *21*, 5601−5606.
(15) Babar, S.; Li, T. T.; Abelson, J. R. Role of nucleation layer morphology in determining the statistical roughness of CVD-grown thin films. *J. Vac. Sci. Technol. A* **2014**, *32*, 060601.
(16) Girolami, G. S.; Jensen, J. A.; Gozum, J. E.; Pollina, D. M. Tailored organometallics as low-temperature CVD precursors to thin films. *MRS Online Proc. Libr.* **1988**, *121*, 429.
(17) Jensen, J. A.; Gozum, J. E.; Pollina, D. M.; Girolami, G. S. Titanium, zirconium, and hafnium tetrahydroborates as "tailored" CVD precursors for metal diboride thin films. *J. Am. Chem. Soc.* **1988**, *110*, 1643−1644.
(18) Yang, Y.; Abelson, J. R. Epitaxial growth of HfB_2 (0001) on Si (001) by etching through a SiO_2 layer. *J. Cryst. Growth* **2008**, *310*, 3197−3202.
(19) Chowdhury, S.; Polychronopoulou, K.; Cloud, A.; Abelson, J. R.; Polycarpou, A. A. Nanomechanical and nanotribological behaviors of hafnium boride thin films. *Thin Solid Films* **2015**, *595*, 84−91.
(20) Chatterjee, A.; Jayaraman, S.; Kumar, N.; Abelson, J. R.; Bellon, P.; Polycarpou, A. A.; Chevalier, J. P. Tribological behavior of hafnium diboride thin films. *Surf. Coating. Technol.* **2006**, *201*, 4317−4322.
(21) de Graaf, A.; van Deelen, J.; Poodt, P.; van Mol, T.; Spee, K.; Grob, F.; Kuypers, A. Development of atmospheric pressure CVD processes for highquality transparent conductive oxides. *Energy Procedia* **2010**, *2*, 41−48.
(22) Lim, S.; Choi, B.; Min, Y.-s.; Kim, D.; Yoon, I.; Lee, S. S.; Lee, I.-M. A study on the development of CVD precursors V−syntheses and characterization of new N-alkoxy-β-ketoiminate complexes of titanium. *J. Organomet. Chem.* **2004**, *689*, 224−237.
(23) Devi, A. 'Old Chemistries' for new applications: Perspectives for development of precursors for MOCVD and ALD applications. *Coord. Chem. Rev.* **2013**, *257*, 3332−3384.
(24) Lawson, J. W.; Bauschlicher, C. W., Jr; Daw, M. S. Ab initio computations of electronic, mechanical, and thermal properties of ZrB_2 and HfB_2. *J. Am. Ceram. Soc.* **2011**, *94*, 3494−3499.
(25) Zhang, J.-D.; Cheng, X.-L.; Li, D.-H. First-principles study of the elastic and thermodynamic properties of HfB_2 with AlB_2 structure under high pressure. *J. Alloys Compd.* **2011**, *509*, 9577−9582.
(26) Sitler, S. J.; Raja, K. S.; Charit, I. ZrB_2-HfB_2 solid solutions as electrode materials for hydrogen reaction in acidic and basic solutions. *Mater. Lett.* **2017**, *188*, 239−243.
(27) Nakamori, Y.; Miwa, K.; Ninomiya, A.; Li, H.; Ohba, N.; Towata, S.-i.; Züttel, A.; Orimo, S.-i. Correlation between thermodynamical stabilities of metal borohydrides and cation electronegativites: First-principles calculations and experiments. *Phys. Rev. B* **2006**, *74*, 045126.
(28) Singh, R.; Trenary, M.; Tanaka, T.; Sen, P.; Batra, I. P. Formation of an ordered Si dimer structure on HfB_2 (0001). *Phys. Rev. B: Condens. Matter Mater. Phys.* **2002**, *66*, 155416.
(29) Hayami, W.; Aizawa, T.; Tanaka, T.; Otani, S. Theoretical Study of the Electronic Structures of HfB_2 (0001)-X (X= Li− Ne) Surfaces. *J. Phys. Chem. B* **2004**, *108*, 15233−15237.
(30) Haaland, A.; Shorokhov, D. J.; Tutukin, A. V.; Volden, H. V.; Swang, O.; McGrady, G. S.; Kaltsoyannis, N.; Downs, A. J.; Tang, C. Y.; Turner, J. F. C. Molecular structures of two metal tetrakis (tetrahydroborates), $Zr(BH_4)_4$ and $U(BH_4)_4$: Equilibrium conformations and barriers to internal rotation of the triply bridging BH_4 groups. *Inorg. Chem.* **2002**, *41*, 6646−6655.
(31) Borisenko, K. B.; Downs, A. J.; Robertson, H. E.; Rankin, D. W. H.; Tang, C. Y. Molecular structure of Hf $(BH_4)_4$ investigated by quantum mechanical calculations and gas-phase electron diffraction. *Dalton Trans.* **2004**, 967−970.
(32) Green, J. C.; de Simone, M.; Coreno, M.; Jones, A.; Pritchard, H. M. I.; McGrady, G. S. Electronic Structure of M $(BH_4)_4$, M= Zr, Hf, and U, by Variable Photon-Energy Photoelectron Spectroscopy and Density Functional Calculations. *Inorg. Chem.* **2005**, *44*, 7781−7793.
(33) Jayaraman, S.; Yang, Y.; Kim, D. Y.; Girolami, G. S.; Abelson, J. R. Hafnium diboride thin films by chemical vapor deposition from a single source precursor. *J. Vac. Sci. Technol.* **2005**, *23*, 1619−1625.
(34) Chan, W. T. K.; Wong, W.-T. A brief introduction to transition metals in unusual oxidation states. *Polyhedron* **2013**, *52*, 43−61.

https://doi.org/10.1021/acsomega.1c00391
ACS Omega 2021, 6, 11404−11410

(35) Morse, P. M.; Shelby, Q. D.; Kim, D. Y.; Girolami, G. S. Ethylene Complexes of the Early Transition Metals: Crystal Structures of $[HfEt_4(C_2H_4)^{2-}]$ and the Negative-Oxidation-State Species $[TaHEt(C_2H_4)_3^{3-}]$ and $[WH(C_2H_4)_4^{3-}]$. *Organometallics* **2008**, *27*, 984−993.
(36) Chen, H.; Andersson, P.; Lindahl, A. O.; Hanstorp, D. The electronic structure of HfF5-and WF5. *Chem. Phys. Lett.* **2011**, *511*, 196−200.
(37) Gnedenkov, S. V.; Sinebryukhov, S. L.; Zheleznov, V. V.; Opra, D. P.; Voit, E. I.; Modin, E. B.; Sokolov, A. A.; Yu Ustinov, A.; Sergienko, V. I. Effect of Hf-doping on electrochemical performance of anatase TiO2 as an anode material for lithium storage. *R. Soc. Open Sci.* **2018**, *5*, 171811.
(38) Niinistö, J.; Putkonen, M.; Niinistö, L.; Song, F.; Williams, P.; Heys, P. N.; Odedra, R. Atomic layer deposition of HfO2 thin films exploiting novel cyclopentadienyl precursors at high temperatures. *Chem. Mater.* **2007**, *19*, 3319−3324.
(39) Williams, P. A.; Roberts, J. L.; Jones, A. C.; Chalker, P. R.; Tobin, N. L.; Bickley, J. F.; Davies, H. O.; Smith, L. M.; Leedham, T. J. Novel mononuclear alkoxide precursors for the MOCVD of ZrO2 and HfO2 thin films. *Chem. Vap. Deposition* **2002**, *8*, 163−170.
(40) Froese, R. D. J.; Hustad, P. D.; Kuhlman, R. L.; Wenzel, T. T. Mechanism of Activation of a Hafnium Pyridyl− Amide Olefin Polymerization Catalyst: Ligand Modification by Monomer. *J. Am. Chem. Soc.* **2007**, *129*, 7831−7840.
(41) Chen, W.; Sun, Q.-Q.; Xu, M.; Ding, S.-J.; Zhang, D. W.; Wang, L.-K. Atomic layer deposition of hafnium oxide from tetrakis (ethylmethylamino) hafnium and water precursors. *J. Phys. Chem. C* **2007**, *111*, 6495−6499.
(42) Niinistö, J.; Mäntymäki, M.; Kukli, K.; Costelle, L.; Puukilainen, E.; Ritala, M.; Leskelä, M. Growth and phase stabilization of HfO2 thin films by ALD using novel precursors. *J. Cryst. Growth* **2010**, *312*, 245−249.
(43) Hsieh, K.-C.; Lee, W.-Y.; Lai, C.-L.; Hu, C.-H.; Lee, H. M.; Huang, J.-H.; Peng, S.-M.; Lee, G.-H. Insertion reactions of phenyl isocyanate into hafnium nitrogen bonds: synthesis and reactivity of hafnium complexes bearing substituted pyrrolyl ligands. *J. Organomet. Chem.* **2004**, *689*, 3362−3369.
(44) Frisch, M.; Trucks, G.; Schlegel, H.; Scuseria, G.; Robb, M.; Cheeseman, J.; Scalmani, G.; Barone, V.; Mennucci, B.; Petersson, G. *Gaussian 09*, Revision, A. 1, 2009.
(45) Perdew, J. P.; Burke, K.; Ernzerhof, M. Generalized gradient approximation made simple. *Phys. Rev. Lett.* **1996**, *77*, 3865.
(46) Adamo, C.; Barone, V. Toward reliable density functional methods without adjustable parameters: The PBE0 model. *J. Chem. Phys.* **1999**, *110*, 6158−6170.
(47) Hay, P. J.; Wadt, W. R. Ab initio effective core potentials for molecular calculations. Potentials for the transition metal atoms Sc to Hg. *J. Chem. Phys.* **1985**, *82*, 270−283.
(48) Boyle, T. J.; Farrell, J.; Yonemoto, D. T.; Sears, J. M.; Rimsza, J. M.; Perales, D.; Bell, N. S.; Cramer, R. E.; Treadwell, L. J.; Renehan, P.; Adams, C. J.; Bender, M. T.; Crowley, W. Synthesis, Characterization, and Nanomaterials Generated from 6, 6′-(((2-Hydroxyethyl) azanediyl) bis (methylene)) bis (2, 4-di-tert-butylphenol) Modified Group 4 Metal Alkoxides. *Inorg. Chem.* **2018**, *57*, 11264−11274.
(49) Module, F. *Material Studio 6.0*; Accelrys Inc.: San Diego, CA, 2011.
(50) Zhan, C.-G.; Nichols, J. A.; Dixon, D. A. Ionization potential, electron affinity, electronegativity, hardness, and electron excitation energy: molecular properties from density functional theory orbital energies. *J. Phys. Chem. A* **2003**, *107*, 4184−4195.

https://doi.org/10.1021/acsomega.1c00391
ACS Omega 2021, 6, 11404−11410